NRL Memorandum Report 4256

Collective Acceleration of Electrons Using an Autoacceleration Process

THOMAS R. LOCKNER

JAYCOR
Alexandria, Virginia 22304

AND

MOSHE FRIEDMAN

Plasma Physics Division

July 11, 1980

This research was sponsored by Defense Advanced Research Projects Agency (DoD)
ARPA Order No. 3718 under contract N60921-80-WR-W0190.

NAVAL RESEARCH LABORATORY
Washington, D.C.

SECURITY CLASSIFICATION OF THIS PAGE (When Data Entered)

REPORT DOCUMENTATION PAGE

READ INSTRUCTIONS BEFORE COMPLETING FORM

1. REPORT NUMBER: NRL Memorandum Report 4256

2. GOVT ACCESSION NO.: AD-A087 001

3. RECIPIENT'S CATALOG NUMBER:

4. TITLE (and Subtitle): COLLECTIVE ACCELERATION OF ELECTRONS USING AN AUTOACCELERATION PROCESS

5. TYPE OF REPORT & PERIOD COVERED: Interim report on a continuing NRL problem.

6. PERFORMING ORG. REPORT NUMBER:

7. AUTHOR(s): T.R. Lockner* and M. Friedman

8. CONTRACT OR GRANT NUMBER(s): ARPA Order-3718

9. PERFORMING ORGANIZATION NAME AND ADDRESS: Naval Research Laboratory, Washington, D.C. 20375

10. PROGRAM ELEMENT, PROJECT, TASK AREA & WORK UNIT NUMBERS: 61101E; 67-0854-0-0

11. CONTROLLING OFFICE NAME AND ADDRESS: Defense Advanced Research Projects Agency, Arlington, Virginia 22209

12. REPORT DATE: July 11, 1980

13. NUMBER OF PAGES: 30

14. MONITORING AGENCY NAME & ADDRESS (if different from Controlling Office): Naval Surface Weapons Center, Silver Spring, Maryland 20910

15. SECURITY CLASS. (of this report): UNCLASSIFIED

15a. DECLASSIFICATION/DOWNGRADING SCHEDULE:

16. DISTRIBUTION STATEMENT (of this Report)

NRL-MR-4256

Approved for public release; distribution unlimited.

17. DISTRIBUTION STATEMENT (of the abstract entered in Block 20, if different from Report)

SBIE

AD-E000 494

18. SUPPLEMENTARY NOTES

*Present address: JAYCOR, Alexandria, Virginia 22304.

This research was sponsored by Defense Advanced Research Projects Agency (DoD) ARPA Order No. 3718 under contract N60921-80-WR-W0190.

19. KEY WORDS (Continue on reverse side if necessary and identify by block number)

Accelerator
Collective accelerator
Propagation
Transmission line
X-ray
Faraday cup

20. ABSTRACT (Continue on reverse side if necessary and identify by block number)

A means of collectively accelerating an intense electron beam is demonstrated. A long pulse (800ns) electron beam is propagated through cavity structures which redistributed the energy in the beam such that most of the beam energy is transferred to a short segment (6 nsec) in the tail of the bram; Electrons are accelerated in a two cavity system from 200 KeV to energies of 2.4 - 3.0 MeV at a beam current of ~ 8 kA. The extension of this principle to larger number of cavitites appears feasible.

DD FORM 1 JAN 73 1473 EDITION OF 1 NOV 65 IS OBSOLETE
S/N 0102-LF-014-6601

SECURITY CLASSIFICATION OF THIS PAGE (When Data Entered)

251950

CONTENTS

COLLECTIVE ACCELERATION OF ELECTRONS USING AN AUTOACCELERATION PROCESS

INTRODUCTION

The generation of high current relativistic electron beams with particle energy of few MeV is now common technology and has been discussed extensively in the literature.[1-4] Methods of generating intense relativistic electron beams (IREB) with particle energies exceeding 10 MeV involve solving complex physics, engineering and financial problems.[5] A potentially simple approach of generating a high kinetic energy electron beam is to use an autoacceleration process[6-14] on a lower voltage electron beam. The autoacceleration process is a collective acceleration mechanism that redistributes the energy within an electron beam such that the majority of the electrons transfer their energy to only a small portion of the beam.

The autoaccelerator described in this paper is a collective accelerator which stores the energy from a long pulse electron beam in coaxial cavities connected to the beam drift tube and deposits this energy to a small portion of the beam at the end of the pulse. Previous experiments have demonstrated this principle at lower energies[10] and with shorter pulse duration.[7] This is the first experiment to demonstrate the autoacceleration mechanism first proposed by Bashmakov et al.[8] at the power levels necessary for the development of a high current high energy accelerator.

Manuscript submitted April 23, 1980.

The principle of operation of the autoaccelerator is shown in Fig. 1. An electron beam is propagated along a strong axial magnetic field in a conducting drift tube at low pressure so that the beam is neither current nor charge neutralized. The drift tube is connected to N coaxial cavities via accelerating gaps as shown in Fig. 1a. The injector current (I_{inj}) and voltage (V_{inj}) rise linearly for a time T to a maximum value I_p and V_p respectively. Because the beam is not current neutralized the return current is forced to flow along the cavity walls 'loading' them with magnetic field energy. The energy stored in the cavity is removed from the electron beam via a decelerating voltage that appears across the gap equal to L dI_b/dt where L is the cavity inductance and I_b is the beam current propagating through the gap. At time T the beam current $I_b(t)$ is forced to drop. For $t > T$ the beam current is down by a factor $\alpha(t)$ from its peak current I_p,

$$\alpha(t) = \frac{I_b(t)}{I_p} \qquad T < t \; . \tag{1}$$

The current falls in a time τ_f which is less than the characteristic time of the cavity defined as $\tau_c = \frac{2\ell}{c}$ (the time for a pulse to propagate from one end of the cavity to the other and back) where ℓ is the cavity length and c is the velocity of light. Under this condition ($\tau_f < \tau_c \ll T$) it is appropriate to model the cavity as a transmission line for $t > T$. In the model the transmission line is shorted at one end and driven by a current source equal to the beam current at the opposite end as shown in Fig. 1e. The characteristic impedance of the line is equal to $Z_c = 60 \ln(r_2/r_1)$ (where r_2 and r_1 are the outer and

inner cavity radii respectively). The accelerating voltage across the gap corresponds to the voltage across the current source and is given by

$$V_g = Z_c \left[I_b (t) - I_p \right] = Z_c I_p \left[\alpha(t) - 1 \right] \qquad (2)$$

for $T < t < T + \tau_c$. This time interval will be referred to as the acceleration phase of the current pulse.

Analysis of the total acceleration in a multi-cavity system is simplified if the injected beam remains relativistic during the acceleration phase. Under this assumption, as the beam is accelerated the electron velocity changes by a negligible amount. This implies that the beam current fall is identical at each gap (except for a timeshift due to the propagation time from gap to gap) and likewise the accelerating voltage. The total electron energy at the end of N cavities is then simply

$$E (t) = q \left[N V_g (t) + V_{inj} (t) \right] \quad T < t < T + \tau_c \ . \qquad (3)$$

The response of a single cavity to the current fall can be most easily visualized by assuming $\alpha(t)$ is a step function in time given by

$$\alpha(t) = 1 - (1 - \alpha_o) \mu_o (t - T) \qquad (4)$$

where $\mu_o(t)$ is the unit step function and α_o is a constant defining the magnitude of the current drop. This gives an instantaneous current drop from I_p to $\alpha_o I_p$ at time T and generates a voltage on the gap of

$$V_g = I_p(1 - \alpha_o) \qquad T < t < T + \tau_c \ . \qquad (5)$$

At time T the current drop initiates a wave in the cavity which

propagates from the gap to the end. Here it is reflected and propagates back to the gap. The initial wave propagating from the gap corresponds to an equivalent transmission line voltage of $Z_c I_p (\alpha_o - 1)$ and current of $I_p (\alpha_o - 1)$. The short at the end of the cavity imposes the boundary condition that the transmission line voltage is zero, thus the reflected wave has a voltage amplitude of $Z_c I_p(1 - \alpha)$ and current amplitude of $I_p(\alpha - 1)$. From the time the wave is launched until the reflected wave returns to the gap the accelerating voltage is given by Equation 2. An interesting result of this simple analysis is that if $\alpha_o = 0.5$ the current and voltage in the cavity drop to zero at time $T + \tau_c$. This indicates that there is no residual energy remaining after the acceleration phase and the efficiency of energy transfer from the cavity to the beam is 100%.

There are several advantages of this accelerator over other acceleration schemes. First, the synchronization of the accelerating voltage is done without external switches on each acceleration stage. This simplifies the scaling of the machine to very high energies. Second, the acceleration pulse length is simply determined by the cavity length and remains constant over the entire length of the device as opposed to the mechanism proposed in Reference 7. Third, it has been shown theoretically[17-19] that even at high current levels this accelerator does not suffer from many of the instabilities which plagued earlier autoacceleration schemes. Finally, in principle the accelerated electrons can be monoenergetic over the entire pulse length. This avoids the necessity of energy discrimination in the output pulse.

EXPERIMENTAL CONFIGURATION

In order to study the autoacceleration mechanism the experiment shown in Fig. 2 was constructed. An LC generator with a 1/4 cycle risetime of 900ns. is connected to a foilless (electron beam) diode via a 30 ohm oil transmission line 3.8 meters in length. The generator is capable of producing a peak voltage of 1.5 MV at 50 kA. The current drop at time T is accomplished by connecting the center conductor of the transmission line to ground via eight radial copper sulfate resistors. The connection is made with a self-break oil switch located 1.3 meters from the LC generator. Locating the switch at this position provides 13 ns of temporal isolation between the current fall produced by the switch and any reflected pulses from the LC generator side of the transmission line. The falltime of the switch τ_f = 6 ns is due to the inductance and resistive phase of the current channel in the oil. Falltimes as short as 2 ns have been observed and are attributed to multiple channel breakdown of the gap. The final value of the transmission line voltage after firing the switch is simply the voltage division between the transmission line impedance and the copper sulfate resistors. In normal operation the resistors are adjusted to give a value of $V_f = 0.25\ V_p$.

The foilless diode produces an annular electron beam 3mm thick propagating 2mm from the wall of the drift tube. The diode voltage and current traces are also shown in Fig. 2.

The diode was designed by J. Shipman of NRL to have a characteristic impedance of 30 ohms up to the cathode stalk. The design minimizes the diode inductance which deteriorates the current and voltage falltime.

The electron beam is propagated along a 10 to 15 KG axial magnetic field in a 4.8cm diameter drift tube coupled to one or two coaxial cavities with a characteristic impedance of 70 ohms. The cavities are 90 cm in length with an inner and outer diameter of 5.1 and 16.8 cm respectively. The system base pressure is 6×10^{-6} Torr and all experiments are performed at pressures below 10^{-4} Torr. At this pressure the beam is current unneutralized.

DIAGNOSTICS

The four diagnostics used on the experiment include magnetic probes, electric probes, a hard X-ray detector and a four channel Faraday Cup. Magnetic and electric probes located at various positions in the cavities are monitored on each shot to compare the cavity operation with the operation predicted from transmission line theory. The X-ray detector and Faraday Cup are used to measure the total accelerated beam energy.

A magnetic probe is installed on the outer wall at each end of the cavity. At the gap end the probe normally monitors the beam current flowing in the drift tube at the axial position of the gap. If the electric field on the gap surfaces is large enough to cause significant electron emission during the acceleration phase, the electron current flowing between the gap surfaces will decrease the total current fall in the cavity as measured by the magnetic probe at the wall. This will decrease the accelerating potential across the gap and thus the efficiency of the accelerator. The magnetic probe at the gap is monitored on each shot and the current fall compared with the beam current fall

to determine if the gap is operating properly.

Another magnetic probe is located on the wall of the cavity at the end opposite the gap. This probe measures the magnetic field produced by the current flowing in the shorted end of the cavity, i.e. the current equivalent to I_2 in Fig. 1e. It will be shown in the next section that this current can be derived analytically using the current at the gap as a source for the transmission line analog of Fig. 1e. The calculated current is compared with the current measured with the magnetic probe to determine if the cavity is responding as a perfect transmission line. Both magnetic probe outputs are integrated using passive RC integrators. Because of the shunt capacitance of the resistors and the differing timescales, separate integrators are used to observe the risetime and falltime. Integrators with RC = 10 μs (RC = 1 μs) are used to observe the risetime (falltime).

Two electric probes are installed at the gap end of the cavity, one on the wall which measures the gap voltage, and the second in the gap close to the center conductor of the cavity. The second probe gives the combined electric field from the space charge of the beam and the potential across the gap. In addition, the probe is driven to a large negative potential when primary beam electrons strike it. This indicates if and when primary electrons are striking the gap during the current risetime.

A hard X-ray detector is the major diagnostic for determining the total accelerated beam energy. As shown in the appendix, the X-ray intensity during the acceleration phase relative to the intensity at

t = T is given by

$$X_r(t) = \frac{X(t)}{X_p} = \alpha(t)^{3.8}\left[N\left(\frac{1}{\alpha(t)} - 1\right)\frac{Z_c}{Z_{dt}} + 1\right]^{2.8} \qquad T < t < T + \tau_c \quad (6)$$

where X(t) is the X-ray intensity for $T < t < T + \tau_c$, X_p is the intensity at t = T, Z_{dt} is the drift tube impedance $Z_{dt} = V_{inj}/I_b$, and the other expressions have been defined previously. This equation is used to predict whether the X-ray intensity should increase during the acceleration phase and by what amount. Because X_r (t) is a strong function of $\alpha(t)$, this measurement is very sensitive to small changes in the accelerated electron energy. It is used in conjunction with the magnetic probe at each gap to determine if the cavities are generating the accelerating voltage expected from the current fall.

The total beam energy is also measured by a four channel Faraday Cup located at the end of the drift tube. A carbon plug with four radial slits aligned with the Faraday Cup collectors is placed in front of the diagnostic to lower the beam current to a suitable level. Carbon absorbers of various thicknesses are placed in front of each collector to determine the accelerated electron energy.

RESULTS

When long pulse operation of a foilless diode had been obtained, a single cavity was installed to verify the autoaccelerator mechanism. The magnetic and electric probe measurements on the cavity outer wall agree well with the currents and voltages calculated using the model in Fig. 1e. The response of the model to an impulse of beam current is

found to be

$$V_{g\delta}(t) = \sum_{n=0}^{\infty} (-1)^n Z_c \quad \delta(t - n\tau_c) \tag{7}$$

$$I_{2\delta}(t) = \sum_{n=0}^{\infty} (-1)^n 2 \quad \delta(t - \frac{\tau c}{2} - n\tau_c) \tag{8}$$

where $V_{g\delta}$ and $I_{2\delta}$ are the impulse responses of V_g and I_2 respectively and $\delta(t)$ is a unit impulse at time $t = 0$. Convolution of the current measured at the gap with the appropriate impulse response gives the predicted values of V_g and I_2. In practice the predicted values of V_g and I_2 are generated by digitizing the oscilloscope trace of the gap current and performing a digital convolution with the impulse responses. These results are then compared with the digitized traces of the measured values of V_g and I_2. The results are shown in Fig. 3. The agreement in both the waveform and magnitude of the signals indicates that the cavity is operating as predicted.

Further proof of the acceleration mechanism is obtained from the X-ray measurements on the single cavity experiments. Note that in Equation 10 of the appendix for $Z_{dt} > 35$ ohms no increase in X-ray intensity is predicted. In the experiment, the drift tube impedance rarely goes below 35 ohms. For all of the shots exhibiting $X_r > 1$ the drift tube impedance was less than 35 ohms.

Experiments using a two cavity system demonstrate the scalability of the acceleration mechanism to obtain higher electron energies. An X-ray trace is shown in Fig. 4 from a two cavity shot. For this shot

Equation 2 predicts an increase of a factor of 2.64 over the primary beam X-ray intensity. This is in close agreement with the experimentally observed increase of a factor of 2.6 $\pm$ .15.

A four channel Faraday Cup was used to analyze the accelerated electron energy on several of the two cavity shots. A carbon absorber of different thickness was placed in front of each channel to attenuate electrons with energy less than a range in the absorber. For the shot shown in Fig. 5 the range for the thickest attenuator was 3 MeV, thus the signal on this channel indicates that electrons with energies up to $\sim$ 3 MeV are present. Using the magnetic probe signal in the second cavity to determine the total beam energy gives a value of 2.4 MeV on this shot. There are two possible causes for the discrepancy in energy between the probe prediction and Faraday Cup. First, since electrons with energies less than a range can penetrate the carbon (with significant attenuation) the signal on channel 4 of Fig. 5 may be due to electrons with less energy than 3 MeV. Second, at these current levels the magnetic probes may be in error due to the large dI/dt signal at the probe. Certainly the value of 2.4 MeV given by the probe calculation is a lower limit on the electron energy.

The total accelerated beam current can be deduced from the X-ray and Faraday Cup measurements. Both diagnostics show that within experimental error ($\pm$ 10%) all of the propagating beam current is being accelerated by the two cavities. In addition, single cavity results using a 1.2 meter cavity (τ_c = 8ns) indicate that the accelerating potential does level off for $\tau_f < \tau_c$ as shown in Fig. 6. This implies that for $\tau_f \ll \tau_c$ a monoenergetic beam can be obtained with a total

output current of I_b (t).

Initial results in one and two cavity systems showed that the cavities often developed large amplitude oscillations during the beam risetime. This was attributed to beam noise exciting the cavity at its various harmonics and thus introducing a large energy modulation on the beam. In order to quench these oscillations, carbon resistor chains were installed in the cavity (Fig. 4) to lower the cavity Q from ∿1000 to 15. This reduced the oscillations at the cavity harmonics by more than a factor of 10 to a level barely measurable on the magnetic probe traces. The change in the X-ray oscillographs is shown in Fig. 7. Note that the oscillation amplitude is accentuated in the X-ray signals due to the $E^{2.8}$ power law for the X-ray intensity. The magnetic probe traces show that the beam current modulation is very small and the oscillation on the X-ray signal is due primarily to energy modulation of the beam from oscillations in the cavity.

In addition to lowering the cavity Q and thus the level of oscillations in the cavity, the resistor chains reduce the accelerating voltage below what would be generated by an unloaded cavity. It was determined experimentally that the impulse response of the cavity changed only in magnitude implying a change in the value of the effective cavity impedance (Z_c). A change in the impulse response, aside from the value of Z_c, would have appeared as a discrepancy between the predicted and measured waveforms of V_g and I_2. The agreement between the calculated and measured probe traces in Fig. 3 also confirm that the cavity response is changing only in amplitude with the addition of the resistors for $T < t < T + \tau_c$. For the configuration used in our experiments the

effective Z_c dropped from 70 to 66.5 $\pm$ 1 ohms which leads to less than a 10% drop in accelerating voltage (from Equation 2). This was an acceptable loss considering the gain in signal to noise in the system.

Consistent single cavity operation has been performed at peak currents (I_p) up to 30 kA. The limit is primarily due to the operation of the generator and foilless diode. At this current level approximately 6 kA of electrons are accelerated to energies of 2.0 MeV. In the present experiment consistent operation of the two cavity system is limited to $I_p \lesssim 15$ kA. For most shots above this current level, the falltime in the first cavity remains normal while the falltime in the second cavity lengthens giving a corresponding decrease in total electron acceleration. Prior to the acceleration phase, fast electron current is measured by the electrostatic probe in the gap, indicating that primary beams electrons are striking the gap. We believe that plasma is formed at the gap by the primary electrons which is then a source of electron current across the gap when the beam current falls. This reduces the total current fall in the gap and thus the accelerating potential for the primary electrons.

The fact that the electrons strike the gap late in the current pulse indicates that either the emitted beam radius is increasing in time or the beam is expanding radially in the drift tube as the current increases. The problem of radial expansion should be alleviated by increasing the energy of the charging beam and by using a shorter rise-time.

CONCLUSION

The autoacceleration mechanism has been confirmed experimentally with one and two cavity systems. Magnetic and electric probes in the cavities produce signals consistent with the transmission line theory predictions. X-ray and Faraday Cup measurements indicate that the bulk of the beam electrons are being accelerated to the full predicted energy given by Equation 3. Carbon resistor chains in the cavities have suppressed RF oscillations during the current risetime to an acceptable level for experiments with more cavities. The beam energy has been increased by a factor of 14 from 200 KeV to 2.4 - 3.0 MeV in a two cavity system and experiments with larger numbers of cavities appear feasible.

APPENDIX

The unique nature of the current and energy pulse of the accelerator made it possible to develop a system which determines the beam energy using the Bremsstrahlung X-rays generated when the electrons strike a target in the drift tube. It has been shown[15] that the X-ray intensity on axis for electron impact on a target is proportional to $IqV^{2.8}$, i.e.

$$X = K\ IqV^{2.8} \tag{9}$$

where X is the X-ray intensity, I is the electron current, qV is the electron energy and K is a constant whose value depends on the distance to the target and its composition. This power law was confirmed in the experiment using the primary electron beam interacting with either a carbon or stainless steel target. The voltage and current traces of the generator were digitized and I vs. log V plotted as

shown in Fig. 8. Using this power law, the X-ray intensity at time T relative to the intensity during the acceleration phase is given by

$$X_r = \frac{X}{X_p} = \alpha^{3.8} \left[N\left(\frac{1}{\alpha} - 1\right) \frac{Z_c}{Z_{dt}} + 1 \right]^{2.8} \qquad T < t < T + \tau_c \qquad (10)$$

Here X_r is the X-ray intensity relative to the value at time T i.e. $X_p = X(T)$, $(t) = I_b(t)/I_p$, and Z_{dt} is the drift tube impedance $Z_{dt} = V_{inj}/I_b$.

Fig. 9 shows computer plots for one and two cavities of X_r vs α ($N = 1$, $N = 2$) with Z_{dt} as a parameter and $Z_c = 65$ ohms. Note that for $N = 1$ the drift tube impedance must be below 35 ohms before X_r is above 1.2. This is significant in that experimentally X_r must be > 1.2 to observe a definitive X-ray pulse. Since the drift tube impedance rarely drops below 35 ohms this is an excellent check on the diagnostic. In fact, using a single cavity X-ray pulses were only observed when Z_{dt} was below 35 ohms. Fig. 9 also shows that for $N = 2$, X_r is a strong function of α for $\alpha < 0.4$. In this range the X-ray detector provides a sensitive measure of whether the current fall at the gap of the cavities was the same as the beam current fall.

The analysis of the X-ray signal is based on two assumptions. First, the diode impedance is assumed constant during the current fall. This is a poor assumption since the diode operates in spacecharge limited flow, however the affect on the accuracy of Eq. 3 is small if the diode voltage after the current fall is much less than the total electron energy after acceleration. This is normally the case in the present experiment.

Equation 10 also assumes that all of the beam electrons in the gap during the acceleration phase are accelerated and are not lost before they strike the target. Because of the agreement between the experimental results and the predicted X_r we feel this assumption is adequately justified. If the assumption were not valid the experimental values of X_r would be consistently lower than those predicted by Equation 10.

REFERENCES

1. J. C. Martin, U. S. Patent No. 3344298, Flash X-Ray Tube with Gas Focusing of Beam (Sept. 26, 1967).
2. S. E. Graybill and S. V. Nablo, Applied Physics Letter 8, 18, (1968).
3. J. J. Clark, M. Ury, M. L. Andrews, D. Hammer and S. Linke, In Record of the Tenth Symposium of Electron, Ion and Laser Beam Technology, L. Marton, Ed., San Francisco Press, San Francisco, CA (1969).
4. M. Friedman and M. Ury, Rev Sci Inst. 41, 1334, (1970).
5. J. C. Martin, Private Communication (1971-1977).
6. L. N. Kazanskii, A. V. Klestov and A. N. Lebedev, Atomnaya Energiya 30, 27 (1971).
7. M. Friedman, Phys Rev Letter 31, 1107 (1973) and Annals of the New York Academy of Sciences 251, 299, (1975).
8. U. A. Bashmakov, K. A. Belovintzev, E. G. Bessonov, Ya. A. Vazdik, S. M. Nikolaev and P. A. Cherenkov, Sov. Phys. Tech. Phys. 18, 696, (1973).
9. N. E. Belov, A. V. Kisletsox and A. N. Lebedev, Atomnaya Energiya 36, No. 3, p. 251 (1974).
10. I. A. Grishaev, A. N. Dedik, V. V. Zakutin, I. I. Magda, Yu. V. Tkach and A. M. Shendorovich, Sov. Phys. Tech. Phys. 19, 1087 (1975).
11. I. A. Grishaev and A. M. Shendorovich, Soviet Physics - Technical Physics 17, No. 11, p. 1871 (1973).
12. T. Lockner, J. Siambis and M. Friedman, In the Proc. of the 2nd Int. Topical Conf. on High Power Electron and Ion Beam Research and Technology, Ed. J. A. Nation and R. N. Sudan, Cornell University,

p. 585 (1977).

13. M. Friedman and T. Lockner, Proc. Third Inter. Conf. on Coll. Methods of Accel. (Herwood Academic Publishers, New York 1979).

14. Thomas R. Lockner and Moshe Friedman, IEEE Transactions on Nuclear Science, Vol NS-26, No. 3, p. 4237 (1979).

15. H. W. Koch and J. W. Motz, Rev. Mod. Phys. 31, 4 (October, 1959).

16. Ross E. Hestler et al, The Experimental Test Accelerator, IEEE Transactions on Nuclear Science, Vol NS-26, No. 3, p. 4180 (1979).

17. J. G. Siambis, Physics of Fluids, 19, p. 1784 (1976).

18. J. G. Siambis, Phys. Rev. Letters, 42, No. 24, p. 1617 (1979).

19. J. G. Siambis, IEEE Transactions on Nucl. Sci., Vol NS-26, No. 3, p. 3610 (1979).

20. J. G. Siambis and M. Friedman, Particle Accel. 8, 217 (1978).

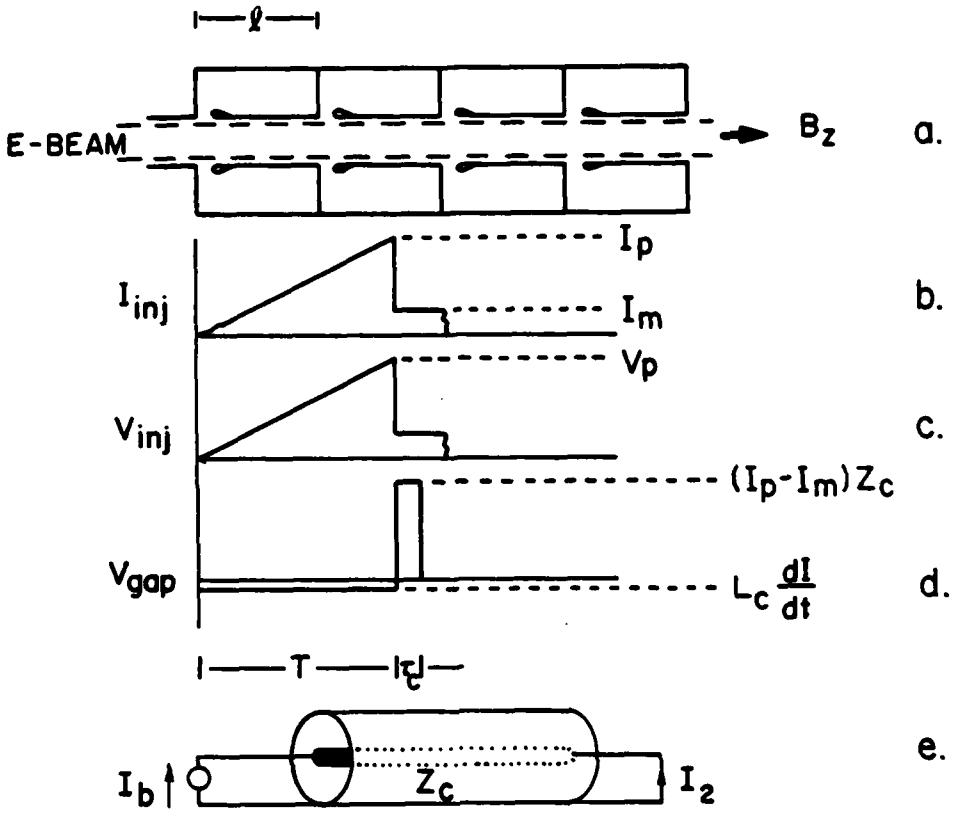

T = CURRENT RISETIME = 800ns

$\tau_c = \frac{2\ell}{c}$ = 6ns

Z_c = CAVITY IMPEDANCE = 70 Ω

L_c = CAVITY INDUCTANCE = 0.23 μh

Fig. 1 — Principle of operation:

a. Electron beam propagation through cavity structures.
b. Injected beam current.
c. Injector voltage.
d. Voltage developed across gap.
e. Transmission line model of cavity for $t > T$.

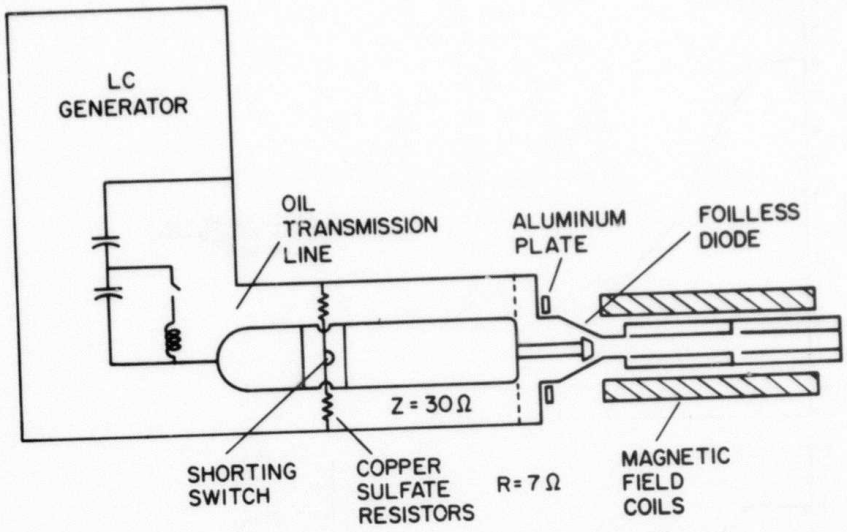

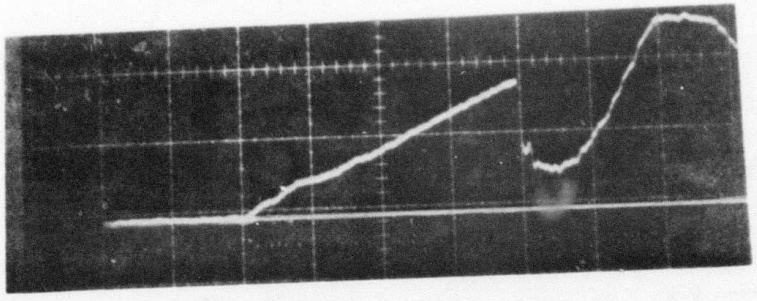

DIODE CURRENT
23 kA/div 200nsec/div

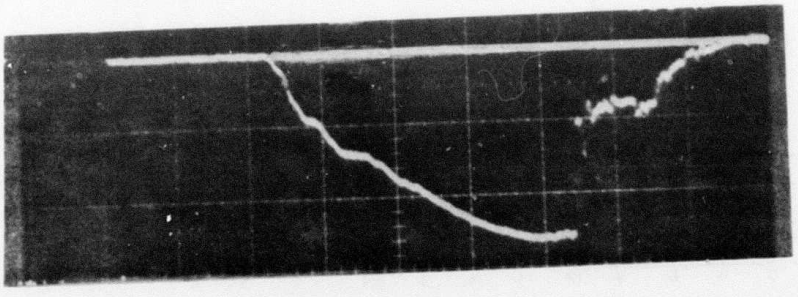

DIODE VOLTAGE
315 kV/div 200nsec/div

Fig. 2 — Experimental configuration

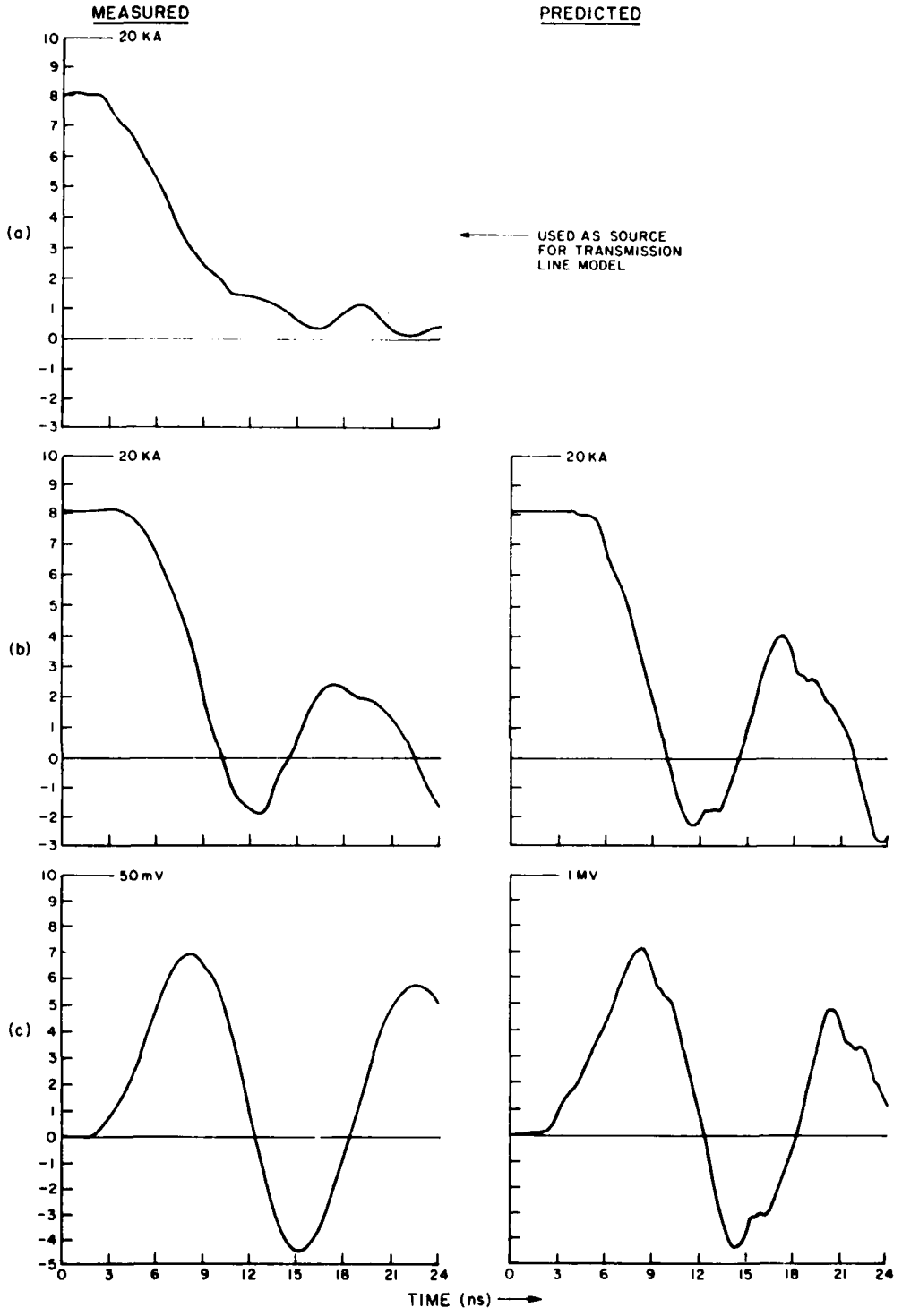

Fig. 3 — Comparison of measured voltage and current in the cavity with simulated traces using the equivalent circuit of Figure 1e. On the left are the measured (a) current at the gap, (b) current at the end, (c) voltage on the gap (not calibrated). The current of (a) is used as a source in the circuit of 1e to generate the traces on the right.

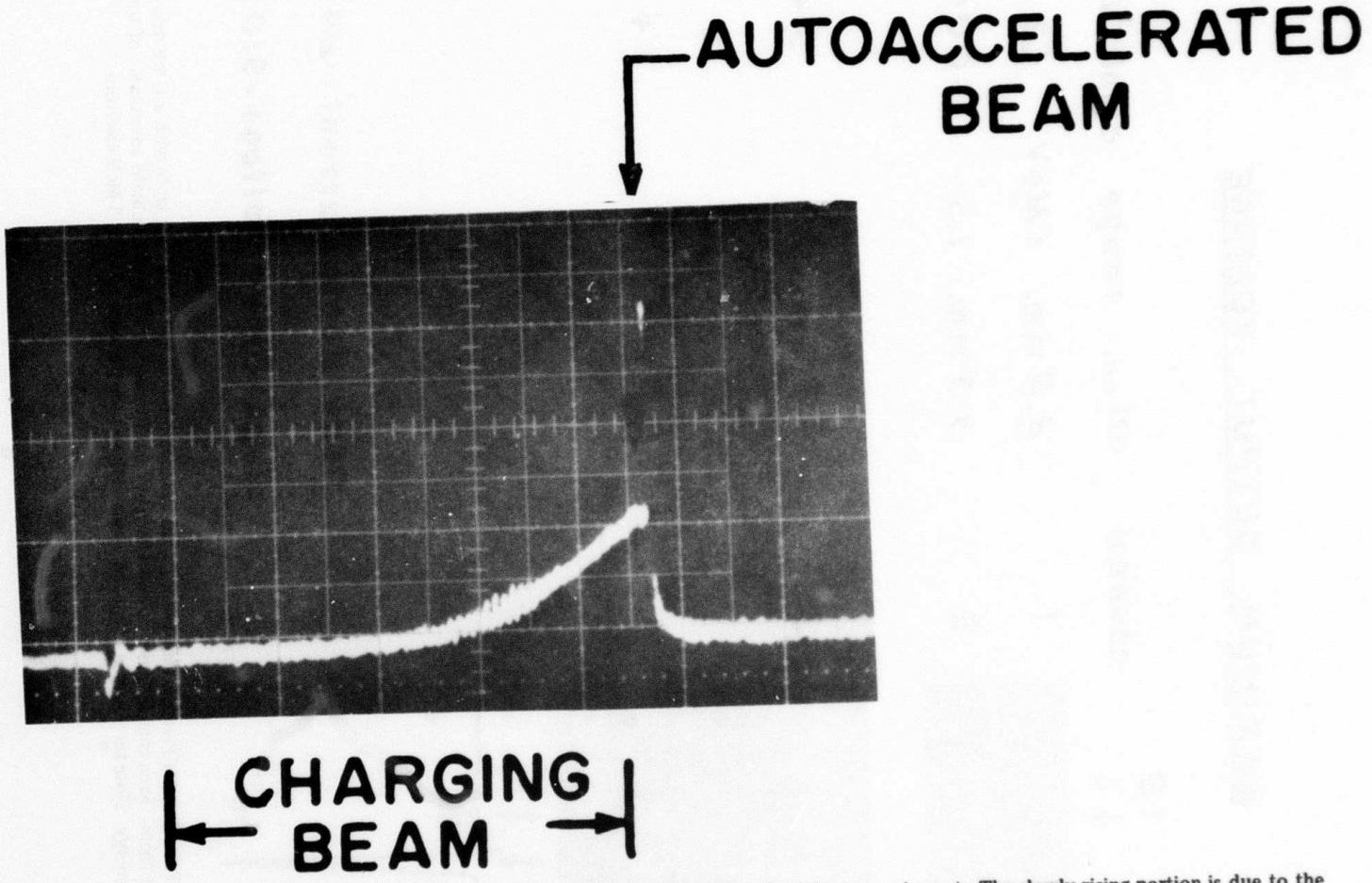

Fig. 4 — Trace of X-ray intensity from beam striking the drift tube wall at the end of the experiment. The slowly rising portion is due to the primary beam. The narrow pulse at the end is from the acceleration of the beam during the current fall. The amplitude of the narrow pulse relative to the peak amplitude of the charging beam agree well with the predicted value.

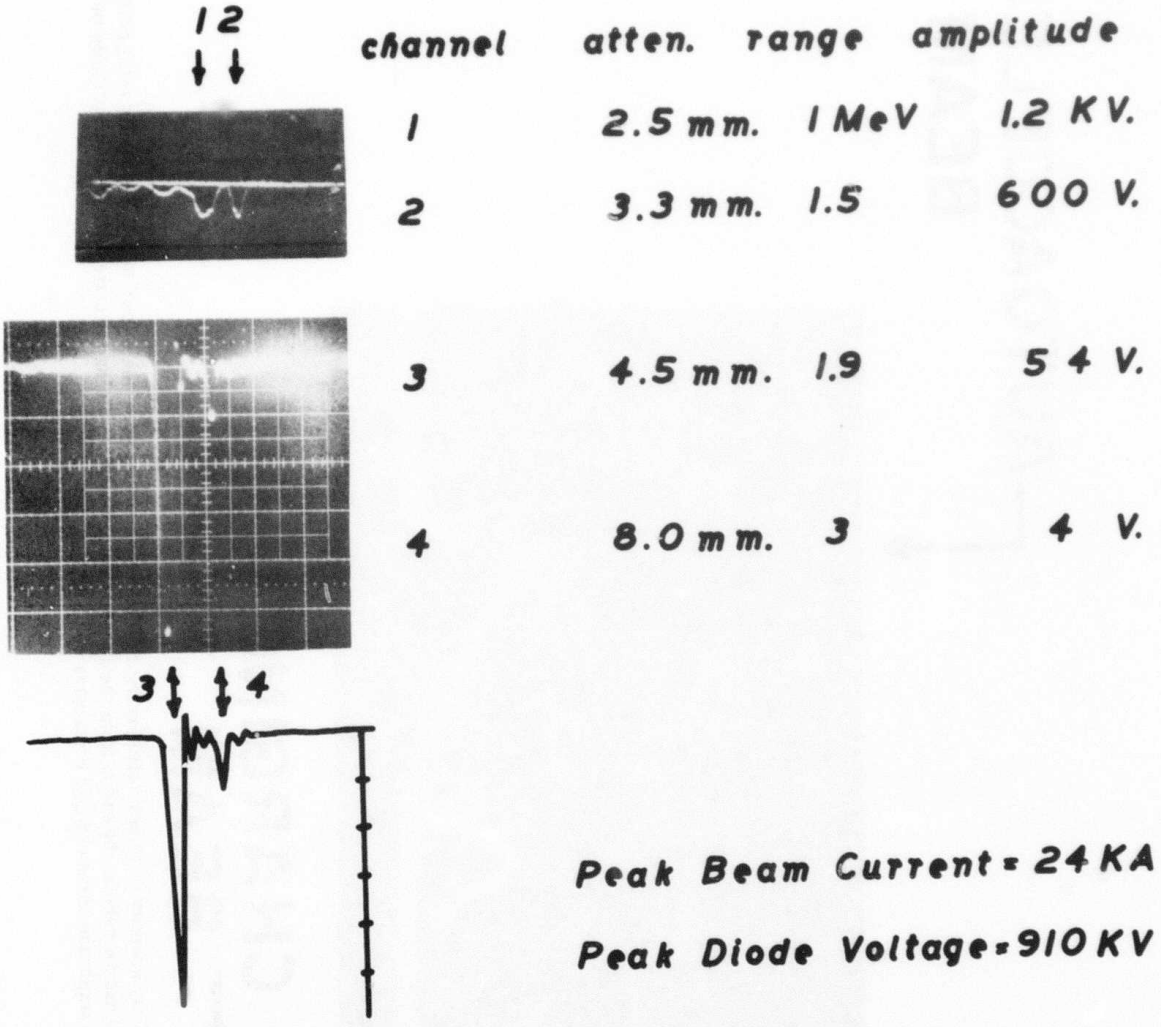

Fig. 5 — Four Channel Faraday Cup Result. Two channels are combined on each trace with a time delay between them. Each channel has a carbon absorber of different thickness to obtain an estimate of the electron energy. Note the signal in channel 4 which indicates the presence of up to 3 MeV electrons.

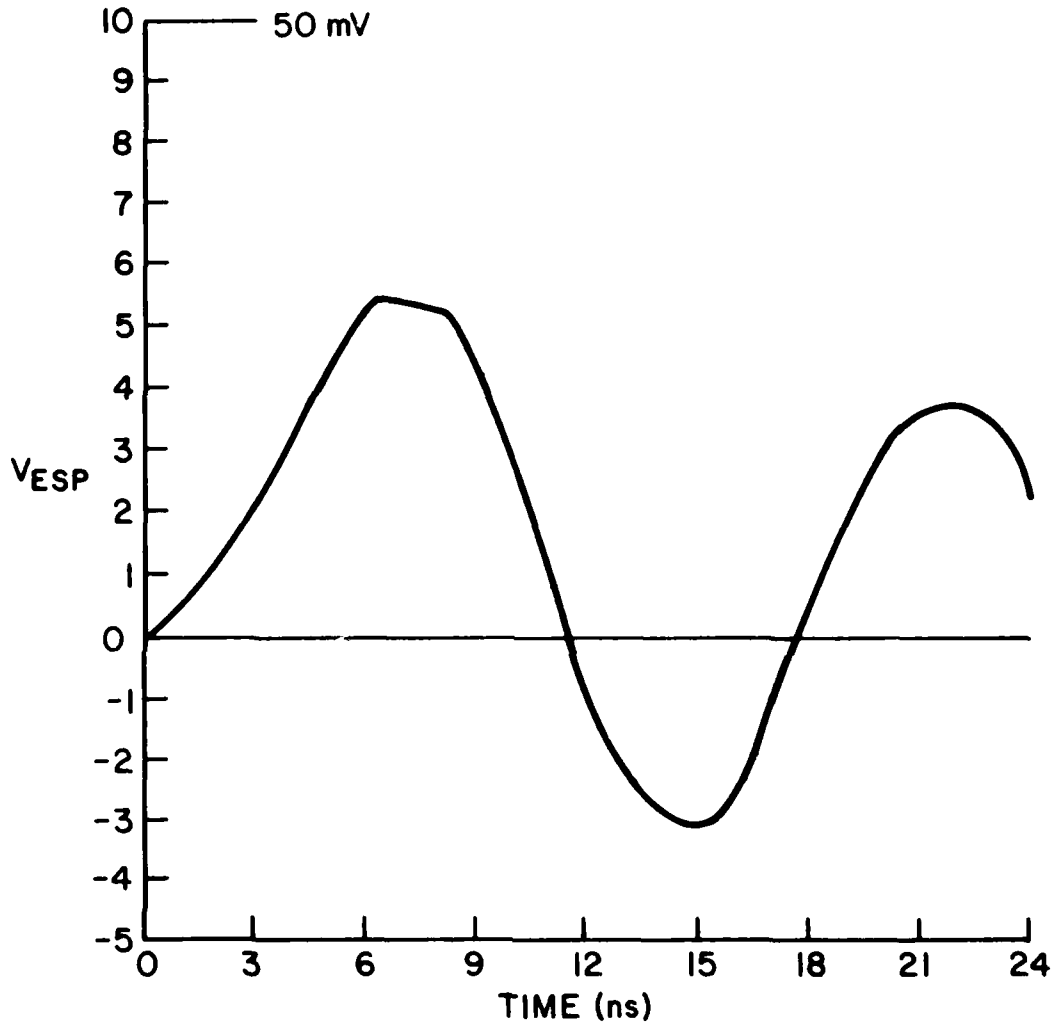

Fig. 6 — Single Cavity Electrostatic probe trace for a 1.2 meter cavity. For this cavity τ_c = 8 ns and τ_f = 6 ns thus $\tau_c > \tau_f$ giving the observed flattop on the probe trace.

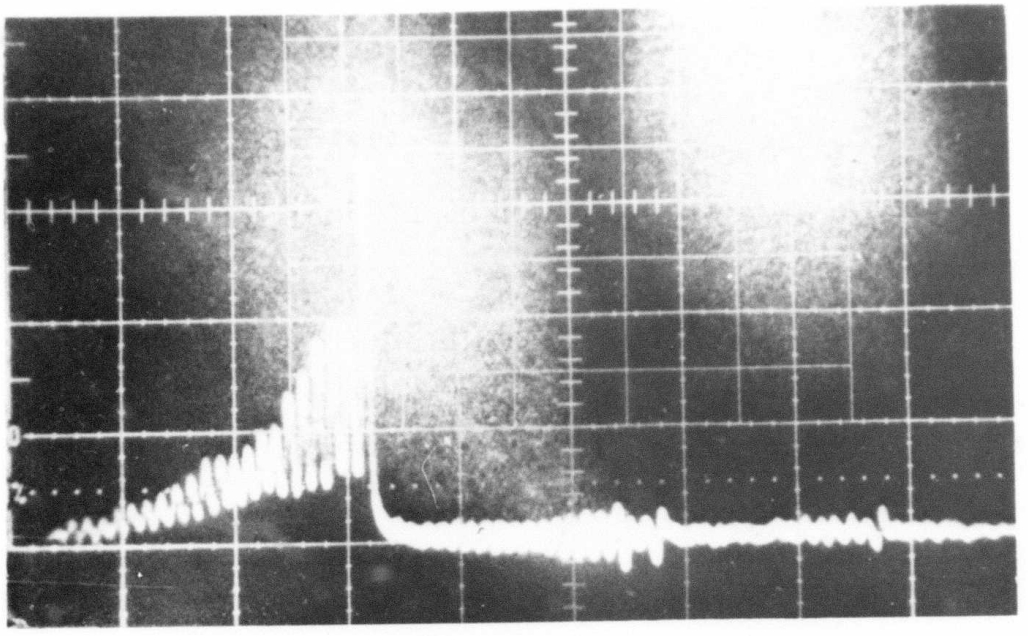

HIGH Q

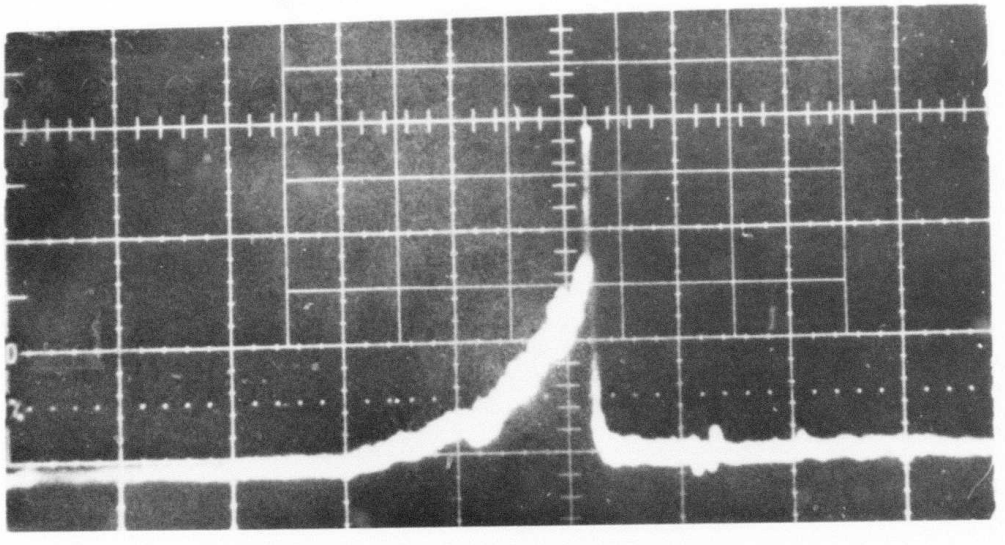

LOW Q

Fig. 7 — X-ray trace showing the effect of the addition of resistor chains to the cavity. Time scale is 200 ns/div. Note the oscillation at the first cavity harmonic which is quenched when the Q is lowered.

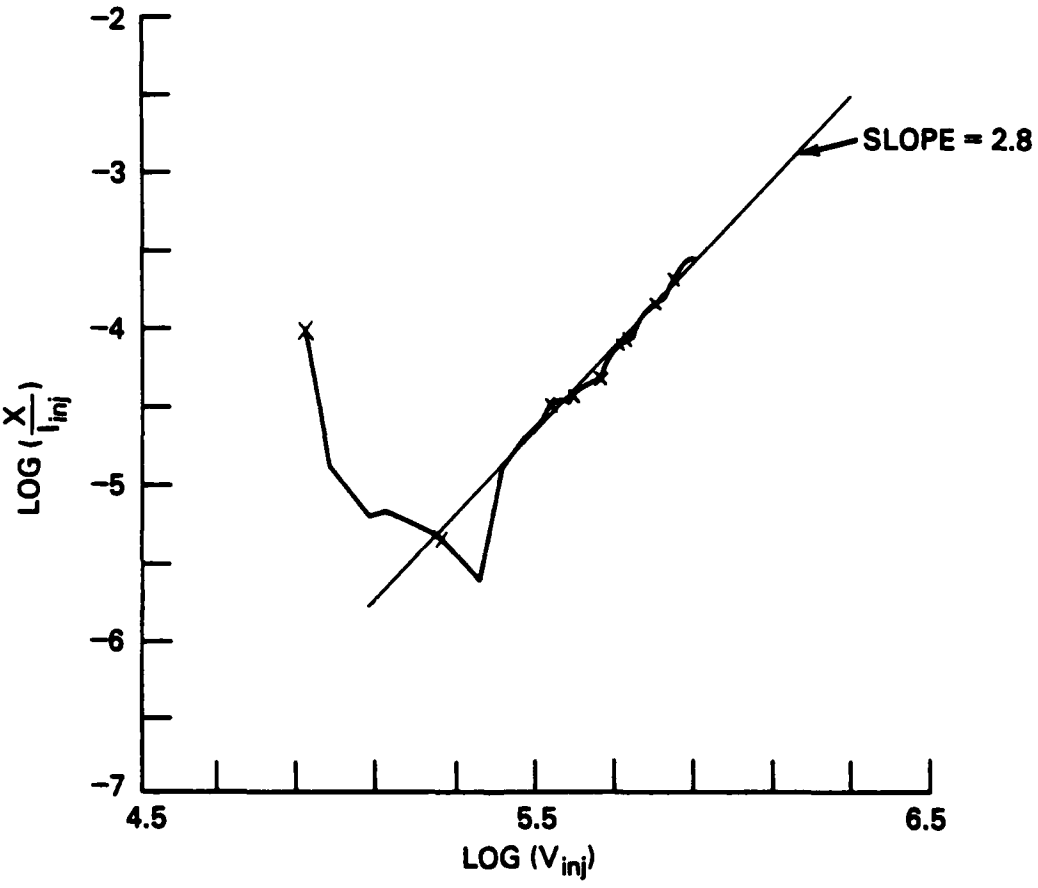

Fig. 8 — Log plot of injector voltage vs. X-ray intensity divided by injector current for one shot. Each cross corresponds to a 60-ns interval.

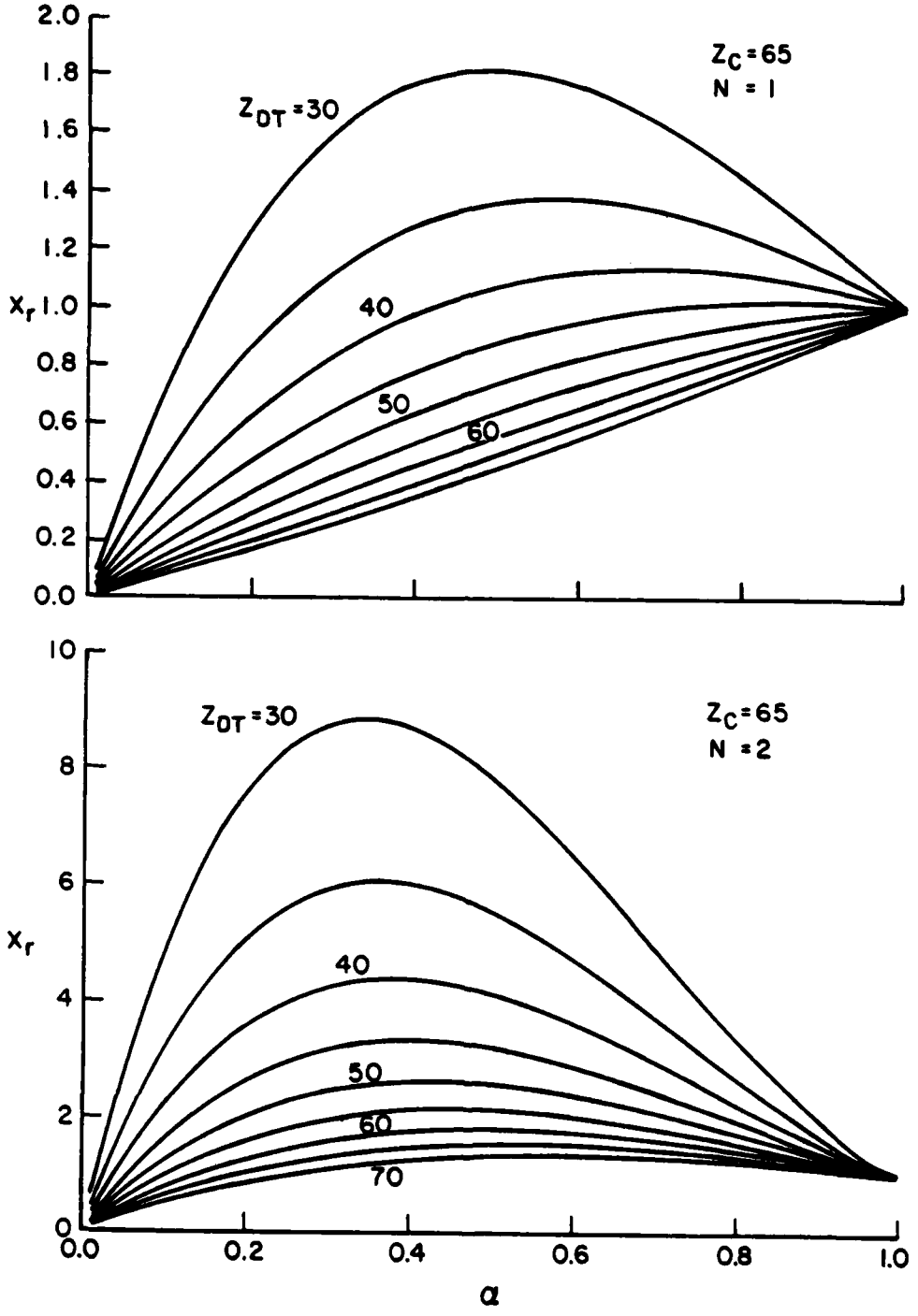

Fig. 9 — Computer plots of Eq. 10. These curves are used to determine the expected increase in X-ray intensity during the acceleration phase as seen in Figure 4.

DISTRIBUTION LIST

1. Defense Technical Information Center — 12 copies
   Cameron Station
   5010 Duke Street
   Alexandria, VA 22314

2. Simon Kassel
   Rand Corp.
   2100 M. St., NW
   Washington, DC 20037

3. Lawrence Berkley Laboratory
   Berkeley, CA 94720
   Attn: D. Keefe
   A. Faltens

4. Lawrence Livermore Laboratories
   University of California
   P. O. Box 809
   Livermore, CA 94550
   Attn: R. Briggs
   L. Reginato
   E. Lee
   D. Fromme
   W. Chapin
   B. Kulke
   W. Barletta
   T. Fessenden
   H. W. Kruger

5. Dr. James Leiss
   Associate Director Office High Energy
   and Nuclear Physics
   Office of Energy Research
   Department of Energy
   MS J309
   Washington, DC 20545

6. Maxwell Laboratories
   9244 Balboa Ave.
   San Diego, CA 92123
   Attn: A. Kolb

7. COMMANDING OFFICER
Naval Research Laboratory
Washington, DC 20375
Attn: Code 4700, Division Superintendent — 25 copies
Code 4701, Jack D. Brown
Code 4700.1, Dr. Moshe Friedman — 20 copies

8. COMMANDER
Naval Surface Weapons Center
White Oak Laboratory
Silver Spring, MD 20910
Attn: R. A. Smith
C. Lyons
C. Huddleston
J. Peters
J. Forbes
Code X211 — 13 copies

9. Physics International
2700 Merced St.
San Leandro, CA 94577
Attn: S. Putnam

10. Dr. M. F. Rose
Naval Surface Weapons Center
Code F102
Dahlgren, VA 22448

11. Harry Diamond Laboratories
2800 Powder Mill Rd.
Adelphi, MD 20783
Attn: P. A. Caldwell
S. Graybill

12. Director
Sandia Laboratories
Albuquerque, NM 87115
Attn: Dr. B. Miller, Fusion
Research Department

13. Ian Smith, Inc.
3115 Gibbons Drive
Alameda, CA 94501
Attn: Dr. I. Smith

14. U.S. Department of Commerce
National Bureau of Standards
Washington, DC 20545
Attn: S. Penner
M. Wilson